Postprint version of the article published in: Journal of Materials Chemistry C, 2019,7, 663-672. https://doi.org/10.1039/C8TC04898C

Journal Name

ARTICLE

Received 00th January 20xx,
Accepted 00th January 20xx

# $Li^+$ and $K^+$ ionic conductivity in non-aligned ionic nematic liquid crystals based on 18-diaza-crown ether substituted with six decylalkoxy-*p*- cyanobiphenyl chains

Verónica Conejo,[a] Cristián Cuerva,[b] Rainer Schmidt,[c] Manuel Bardají,[a,*] and Pablo Espinet[a,*]

**Summary**

Two macrocycles containing six decylalkoxy or decylalkoxy cyanobiphenyl chains symmetrically distributed around a 18-diaza-crown ether core have been prepared. The one with decylalkoxy cyanobiphenyl chains, and their adducts with KI, $K_2[PtCl_4]$, $K[AuCl_4]$, ½ $K[AuCl_4]$, $K_4[Fe(CN)_6]$ or LiI for the second macrocycle, are enantiotropic liquid crystals that display a nematic mesophase with melting points in the range 16.7-29.5 °C and clearing points in the range 86.4 to 98.7 °C. The dielectric permittivity of the complexes has been determined by impedance spectroscopy in the solid, in the mesophase and in the isotropic liquid state, under variable temperature between 160 K and 390 K. The equivalent ionic conductivity of these mesogens in their natural non-aligned mesophases and as isotropic liquids are in the range $4.01 \times 10^{-7}$ to $9.67 \times 10^{-10}$ $Scm^{-1}$ at 350K, and in the range $2.02 \times 10^{-6}$ to $1.64 \times 10^{-8}$ $Scm^{-1}$ at 390K. The maximum conductivity values are obtained for the LiI derivative ($4.01 \times 10^{-7}$ $Scm^{-1}$ at 350K and $2.02 \times 10^{-6}$ $Scm^{-1}$ at 390K) with an activation energy of 0.74 eV. Interestingly, the conductivity in the mesophase for the compound with ½ $K[AuCl_4]$ (diaza-crown-ether:AuK = 2:1) is about 20 times higher than for $K[AuCl_4]$ (diaza-crown-ether:AuK = 2:1), which supports that the presence of vacant diaza-crown-ether sites in the mesogen improves the conductivity for $K^+$. A model of ionic conductivity by $K^+$ or $Li^+$ charge carriers explaining the experimental results as well as the effect of the counteranions is proposed.

**Keywords:** liquid crystals, metallomesogens, crown ether, ionic conductivity.

## Introduction

Ionic liquids (ILs) are usually defined as salts with melting points below 100 °C. They can display properties such as good thermal stability, low vapour pressure, wide liquid range, and ionic conductivity.[1] ILs find use in many fields, from solvents in green chemistry to energy storage and conversion in batteries.[2] Ionic liquid crystals (ILCs) are materials that combine the properties of ILs with those of liquid crystals (LCs): some order, anisotropy, easy processing, spontaneously self-assembling, and self-healing abilities.[3] ILCs have been studied as anisotropic ion-conductive materials due to their anisotropic structural organisation and the presence of ions as charge carriers. The long alkyl chains typical of mesogenic molecules can act as insulating layers in ion conductive materials. Nonetheless ILCs are promising materials for molecular electronics, batteries, fuel cells, and capacitors.[4] Other applications have been proposed in the fields of electrochromic or photoluminescent materials, and as organised media for gas adsorption and chemical reactions.[5] Solubilizing the low cost potassium-ion in non-aqueous media is a requirement for the development of sustainable energy storage technology.[6] Pedersen reported in 1967 crown ethers as macrocyclic ligands in which the cavity size and the number of donor atoms can be tuned to accommodate different metal cations and solubilise them in non-polar organic solvents.[7] There are many studies on thermotropic LCs containing crown ethers that coordinate alkali metal ions.[8] Forming the cation-crown adduct changes, sometimes very notably, the LC behaviour of the original material. For instance, the introduction of alkali salts can generate mesomorphism from non-mesomorphic compounds or induce the formation of more ordered phases. In other cases, only the mesophase range changes, or it is lost.[9,10] The counteranion can be very relevant, and soft anions have been reported to stabilise significantly the mesophases.[11]

Cation-induced aggregation/disaggregation processes in $Rh^I$ metal complexes with ligands bearing crown ethers have allowed for the modulation or induction of $Rh^I \cdots Rh^I$ interactions, with spectral responses that could be used for colorimetric and luminescent cation sensing.[12]

In this paper, we report the synthesis and characterization of neutral symmetric macrocycles formed by a 18-diaza-crown ether core and two aryl groups, affording altogether six alkoxy

[a] *IU CINQUIMA/Química Inorgánica, Facultad de Ciencias, Universidad de Valladolid, E–47071 Valladolid, Spain.*
[b] *Departamento de Química Inorgánica I, Facultad de Ciencias Químicas, Universidad Complutense de Madrid, Ciudad Universitaria, E-28040 Madrid, Spain.*
[c] *GFMC, Departamento de Física de Materiales, Universidad Complutense de Madrid, Ciudad Universitaria, E-28040 Madrid, Spain.*

† Footnotes relating to the title and/or authors should appear here.

Electronic Supplementary Information (ESI) available: [$^1$H NMR spectra, DSC thermograms, X-ray Powder Diffraction patterns]. See DOI: 10.1039/x0xx00000x

lateral substituents, and their use as ligands able to trap potassium cations producing ionic macrocycles with ILC behaviour. These hybrid materials are soluble in organic solvents, and show ionic conductivity in the solid state, in the mesophase, and in the isotropic liquid. Using similar diaza-crown ether cores, organic-metal cluster hybrids with liquid crystalline behaviour, named clustomesogens, have been recently published.[13,14]

## Results and discussion

### Synthesis and structural characterization

Literature methods were used to prepare the neutral macrocycles **1** and **2** (Figure 1),[14a,15] containing six decylalkoxy ($R^1$) or *p*-cyanobiphenyl decylalkoxy ($R^2$) chains. Macrocycles **1** and **2** are air–stable orange or, respectively, yellow solids at room temperature and were characterised by elemental analysis, IR and NMR spectroscopy. The $^1$H NMR spectra display the signals corresponding to aromatic protons (a singlet at 6.57 ppm) and, for **2**, the biphenyl protons (two AA'BB' spin system) partially overlapped as three complex signals centred in the range 7.6–7.0 ppm.[16] The resonances due to the diaza-crown ether methylenes appear as multiplets centred around 3.80 (N-$CH_2$) and 3.60 (O-$CH_2$) ppm. Mass spectra (MALDI-TOF) show the parent peak for each macrocycle.

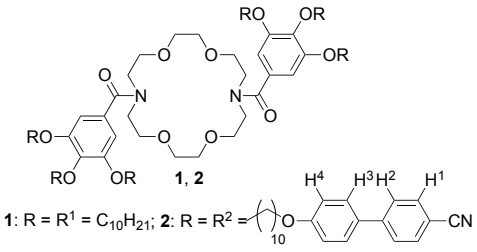


Figure 1. Macrocycles **1** and **2**.

The 18-crown ether cavity in the macrocycles fits well the size of $K^+$, and reaction of these macrocycles with potassium salts, leads to the corresponding host-guest complexes. Potassium salts with different counteranions were made (Scheme 1) in order to study possible changes in liquid crystal, permittivity and ionic conductivity behaviour. Macrocycle **1** was combined with KI, a salt typically used in electrolytes, and with $K_2[PtCl_4]$ but the lack of liquid crystal behaviour of the two compounds moved us to concentrate on macrocycle **2**, which produced liquid crystals in all cases studied. Thus, the presence of the cyanobiphenyl groups is crucial for the mesomorphic behaviour. Salts KI, $K_2[PtCl_4]$, $K[AuCl_4]$, and $K_4[Fe(CN)_6]$ were used to compare different cation/anion stoichiometries 1:1, 2:1 and 4:1. Additionally, a 50% defect of $K[AuCl_4]$ in **2d** allowed us to measure the effect of the presence of non coordinated crown ethers on the ionic conductivity. Finally, 1:1 LiI was also used in **2f** to compare with KI and see the effect of the cation.

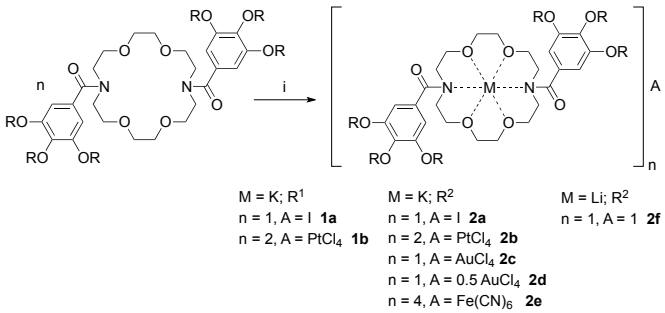


Scheme 1. i) KI (**2a**), $K_2$ $[PtCl_4]$ (**2b**), K[$AuCl_4$](**2c**), ½ K[$AuCl_4$] (**2d**), $K_4[Fe(CN)_6]$ (**2e**) or LiI (**2f**).

Compounds **2a-f** are air–stable solids at room temperature and were characterised (as well as **1a-b**) by elemental analysis, IR, and $^1$H NMR spectroscopy. The IR and $^1$H NMR spectra of the complexes are nearly identical to their parent macrocycle. Mass spectra show the parent peak for each cationic adduct, although mixed with peaks for the protonated macrocycle and for the corresponding sodium adduct. The latter are due to the substrate used to run the MALDI-TOFF experiments, as reported for similar compounds with the same technique.[11c]

### Thermal and mesomorphic behaviour of the compounds

Macrocycle **1** and its **1a** and **1b** adducts are waxy solids that melt to an isotropic liquid at around 50 °C. However, macrocycle **2** and its adducts (compounds **2a**-**2f**) show enantiotropic liquid crystal properties followed, on cooling, by a glass transition, which is maintained in the second heating. The mesomorphic properties of **2**-**2f** were studied by differential scanning calorimetry (DSC) and polarised optical microscopy (POM). The formation of nematic mesophases upon heating and cooling (Figure 2) is in coincidence with the results reported for the same macrocycles but with n = 3 or 9, instead of 10.[13]

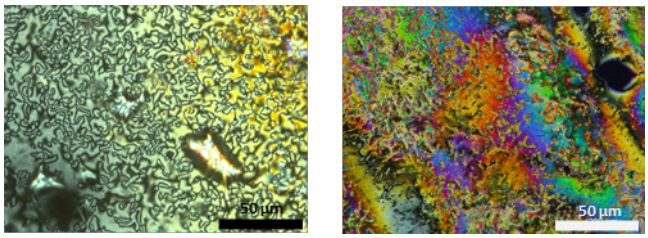


Figure 2. Polarising optical microscopy photographs recorded on cooling from the isotropic phase for compound **2** at 90°C (left), and for **2a** at 67 °C (right).

The phase transition temperatures of **2**-**2f** and their associated enthalpy data are summarised in Table 1. They melt in the range 16.7–29.5 °C to a nematic (N) phase, and their clearing temperatures are in the range 86.4–98.7 °C. Therefore, they are thermotropic liquid crystals at temperatures close to ambient, and in broad temperature ranges (around 70 °C). The melting and clearing points are quite similar for compound **2** and its potassium adducts (less than 5 °C difference), while for the lithium adduct they are around 10 °C lower than for **2**.

Table 1. Optical, thermal, and thermodynamic data of **2** and its **2a**-**2f** adducts.

| Comp. | Transitions[a] | T[b] [°C] | $\Delta C_p$[b] (kJ/g. °C) | $\Delta Hc$[b] (kJ/mol) |
|---|---|---|---|---|
| **2** | g→N | 30.0 | -0.43 | - |
| | N→I | (89.0) 98.8 | | 9.82 |
| **2a** | g→N | 27.2 | -0.35 | - |
| | N→I | (84.4) 94.8 | | 11.11 |
| **2b** | g→N | 25.1 | -0.41 | - |
| | N→I | (83.6) 93.0 | | 22.86 |
| **2c** | g→N | 29.4 | -0.51 | - |
| | N→I | (95.6) 98.6 | | 10.83 |
| **2d** | g→N | 26.5 | -0.23 | - |
| | N→I | (87.4) 94.9 | | 11.84 |
| **2e** | g→N | 27.7 | -0.45 | - |
| | N→I | (84.2) 95.5 | | 45.66 |
| **2f** | g→N | 16.7 | -0.39 | - |
| | N→I | (ovl.) 86.4 | | 9.68 |

[a] g = glass, N = nematic mesophase, I = isotropic liquid. [b] Data taken from the second heating (onset temperatures; maximum temperature in parenthesis of the transition previous to clearing). Heating and cooling at 2 °C/min. Ovl. = overlapped. See text for the value in parenthesis.

All the compounds, including the purely organic molecule **2**, show a complexity in the N→I transition, which seems to occur in two steps usually separated by about 10 °C. The first transition is insinuated only subtly in POM by the appearance of some ribs in the texture. However, the DSC traces reveal clearly their existence, as a relatively low energy transition preceding the real clearing point. It is better observed on 2nd heating and cooling (Figure 3) and is more or less overlapped with the clearing peak, depending on the case.

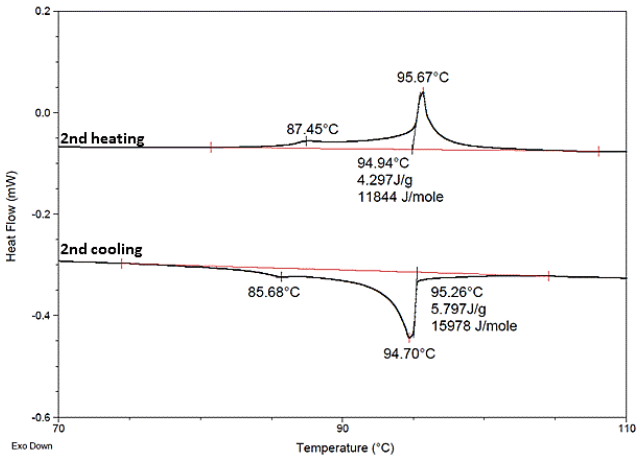


Figure 3. DSC curve for compound **2d**.

The initial transition is indicated in Table 1 by its approximate transition temperature (maximum of the peak) in parenthesis, preceding the clearing temperature (onset point). The calorimetric data cannot be assigned separately and are given for the sum of the two steps. The two phenomena detected calorimetrically overlap over an interval of about 20 °C, which occurs even al low heating ramps of 2 °C/min.

Compounds **2a** and **2f** were selected for powder XRD experiments at variable temperature, in order to assess the molecular arrangement in the mesophase, proposed by POM. XRD experiments between 25 °C and 120 °C show patterns containing broad and diffuse scattering halos, consistent with the proposed nematic nature of all the samples (see Figures S14–S17 in ESI). In the best cases the two-step clearing transition can be guessed from the appearance of some apparent multi-structure in the skyline of the otherwise monotonic curve.

Overall, the liquid crystal behaviour seems to be dominated by the biphenylnitrile moieties with only modest influence of the metal salts, considering that: i) **1** and **1a**, lacking these moieties, are not mesogenic; ii) the organic substrate **2** and the derivatives with $K^+$ or $Li^+$ salts show very similar DSC traces, including the two step clearing, indicating some phenomenon that is generated by the organic molecule; and iii) the interval of melting and clearing points for the whole range of compounds is relatively narrow.

From the data, lamellar structures defining layers are excluded. Although there is no clear evidence to decide whether there is occasional alignment of neighbouring diazo-crown moieties with some ordering defining sort range tunnels, it is statistically obvious that some temporary coincidences cannot be excluded in a fluid material. On the other hand, it is well accepted that $K^+$ has the correct radius to be able to pass through the hole of 18-crown-6 (it is coordinated in an almost planar structure),[17] what we assume also as possible for the equivalent diaza-crown ether **2**. All these parameters define fuzzy sceneries of possibilities for $K^+$ mobility in **2a**-**2f**.

**Conductivity measurements**

The dielectric properties of compounds **2a**-**2f** were studied by impedance spectroscopy in the solid, [18] in the mesophase and in the isotropic liquid state, under variable temperature between 160 K and 390 K. The maximum of 390 K was chosen slightly over the clearing point where the mesophase/liquid phase transition of the ILCs occurs. The minimum of 160 K was chosen well below the onset of any measurable conductivity.

Figures 4a,b show the data for compounds **2a** (KI) and **2f** (LiI) in the notation of Z'' *vs* Z'. The curves show a fully developed semicircle, which corresponds to the charge transport within the material. At the right side of the fully developed semicircle, a fairly straight line ("pike") is visible. This spectral feature is related to ionic charge carriers, which are blocked at the interface (**IF**) between the sample and the electrodes. The ionic charge carriers cannot cross the interface region and move into the metallic electrodes; only electrons could do, in case there was electronic conductivity, which is not the case. Thus, this blocking effect is a hallmark feature of the conductivity observed being ionic. It appears in the mesophase (350 K) and in the liquid state (390 K) of both representative compounds (**2a** and **2f**). The semicircles in each spectrum, related to the ionic conductivity within the material are characterised by their diameter, which corresponds to the resistance of the ionic charge transport. It is evident that the

ILC **2f**, based on lithium iodide, shows a considerably lower resistance (smaller semicircle diameter) than the KI compound **2a**. Since both compounds are otherwise identical and their long range order is equivalent, this difference suggests considerably higher mobility of the $Li^+$ ion, smaller than to $K^+$ (cation diameters: $Li^+$ = 1.46 Å, $K^+$ = 3.04 Å).[9g] In other systems this might be due simply to steric reasons: smaller size leads to lower resistance.[19] Sometimes the contrary is found, in some solvents where the charge carrier density and mobility are expected to be higher for weaker Lewis acids as charge carriers because they interact more weakly with the solvent molecules, as is the case potassium versus lithium ions.[20] In our system it is reasonable to assume that the mobility of the cation must depend on the retention of the cation by the 18-diaza-crown ether, which depends not only on the acidity of the cation, but mostly on a good size match between the 18-crown ether and the cation diameters A good match means that all the heteroatoms in the crown can interact with the cation, providing a higher binding energy. The 18-diaza-crown ether fits well cation diameters in the diameter range 2.6–3.2 Å, which includes $K^+$ but not $Li^+$, so $Li^+$ is less retained than $K^+$.

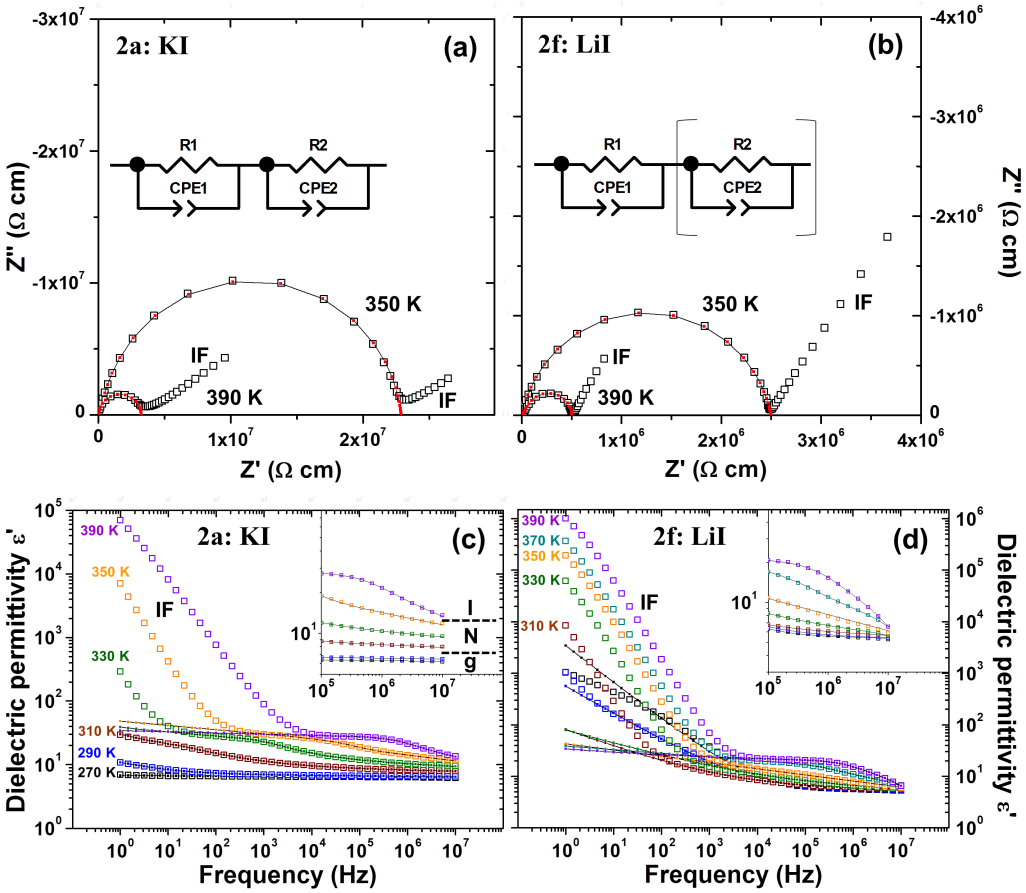


Figure 4. Dielectric data for compounds **2a** and **2f** in the notations of Z'' vs Z' (a & b) and ε' vs *f* (c & d) at selected temperatures as indicated. The figure c & d insets display magnifications of the high *f* data (I: isotropic liquid; N: nematic phase; g: glass). Open symbols represent measured data, solid squares and solid lines correspond to the fitted curves using the equivalent circuit shown in a & b insets.

The fact that **2a** and **2f**, having the same $I^-$ counteranion and only differing in the interaction of the $M^+ = Li^+, K^+$ with the diazacrown moiety, exhibit large differences in conductivity (see later the conductivity plot in Figure 5), suggests that a very significant contribution from the $I^-$ counteranion to the ionic conductivity is unlikely. Moreover, the large anisotropic anions such as $[PtCl_4]^{2-}$ or $[AuCl_4]^{1-}$ do not look prone to move easily in a nematic medium defined essentially by aliphatic and aromatic zones. These considerations point to $Li^+$ and $K^+$ as the charge carriers in the ionic conduction mechanism detected in the mesophase. Figures 4a,b also show, for both cations, distinct decreases in semicircle diameter when the temperature is increased from 350 K (mesophase) to 390 K (isotropic liquid phase). This is the expected result in a thermally activated charge transport mechanism such as ionic conductivity.

Clearer signs of ionic conductivity are observed in the respective plots of dielectric permittivity (ε') versus frequency (*f*) for compounds **2a** and **2f** (Figure 4c,d). At temperatures where compounds **2a** and **2f** are in the mesophase or in the isotropic liquid phase, a large increase of ε' at the low *f* end is observed. This is another typical feature of ionic conductivity, where the high permittivity ε'

is again associated to blocking of the charge carriers at the sample/electrode interface.

The data obtained from all other samples (**2b – 2e**) show, in the Z'' *vs* Z' and in the ε' *vs. f* plots, equivalent features of ionic conduction in the mesophase and in the liquid. It is interesting to note that the distinct "pike" feature in the ε' *vs f* plots is absent in the glass phase, particularly for compound **2a**. This is again in agreement with an ionic conduction mechanism that appears only in the fluid phases (mesophase and isotropic liquid), and may be facilitated by the higher flexibility of the molecular positions and, possibly, by cooperative motions.[21] In Figure 4c,d insets, a magnification of the high *f* data is shown. In the case of compound **2a** (Figure 4c) a clear correlation of the ε' plateau value at high *f* with the phase transitions is observed. At 290 K and all lower temperatures, the data points fall approximately on the same ε' plateau value. However, a clear increase is detected at 310 K, where the compound is transiting into the mesophase (see later). Within the mesophase range, the increase in ε' continues up to the isotropic liquid phase. In this context, it should be noted that the high *f* plateau in ε' *vs. f* data can be associated to the intrinsic dielectric permittivity of the compound. The g → N phase transitions from the glass (g) to the nematic (N) mesophase and the N → I to the isotropic liquid phase are indicated in the inset of Figure 4c by dashed bold lines. This correlation is slightly less clear in **2f** as indicated in the inset of Figure 4d, which may be partially due to the fact that the curves not always reach the *f*-independent plateau value up to the experimental high-*f* limit. The nominal values of the intrinsic permittivity in compounds **2a** and **2f** are around $10^1$, which are relatively low values. However, it should be considered that ε' was calculated from the capacitance and only an estimation of the geometric factor *g* of the samples.

All the dielectric data were fitted to adequate equivalent circuit models consisting of a series connection of two non-ideal resistor–capacitor (RC) elements, as indicated in the insets of Figures 4a,b. The capacitors have been replaced by constant-phase elements (CPE) leading to R-CPE elements (which can be termed RQ elements as well).[18] For compound **2a** at all temperatures, and for compound **2f** in the isotropic liquid phase, two series R-CPE elements were employed, whereas for **2f** in the glass and N mesophase one R-CPE element was sufficient. The use of two series R-CPE elements can be justified by a bimodal distribution of the dielectric relaxation times t, which is evident from the appearance of two plateaus in the ε' *vs f* plots at intermediate and high *f*, as shown in Figure 4a,b. The fits were performed over the full *f* range in the glass phase for both compounds, but only at intermediate and high *f* in the mesophase and in the liquid state. This is because the "pike" feature associated with the sample/electrode interface (**IF**) cannot be accounted for by standard R-CPE elements and a valid fit including the **IF** contribution is therefore not possible. Good agreement between data and fitted curves is indicated in Figure 4a-d in the *f* ranges where a valid fit could be obtained. In the case of two series R-CPE elements in the circuit model, the resistance of the main contribution from the ILCs was taken as R1 + R2, and converted into the resistivity ($\rho$) format considering the approximate sample dimensions in terms of the geometrical factor *g*.

Figure 5 plots the $\sigma$ *vs T* curves for all samples **2a–2f**. The temperature ranges are highlighted indicating the phase transition zones from glass phase to the nematic mesophase (g → N) or from the mesophase to the liquid phase (N → I) occur. As commented above, these zones span about 30 K. The phase transition temperatures deduced from conductivity measurements may be slightly shifted with respect to the DSC data (Table 1) due to the different heating ramps (°C/min) and the different experimental techniques used, where phase transitions may naturally show up at moderately different temperatures.

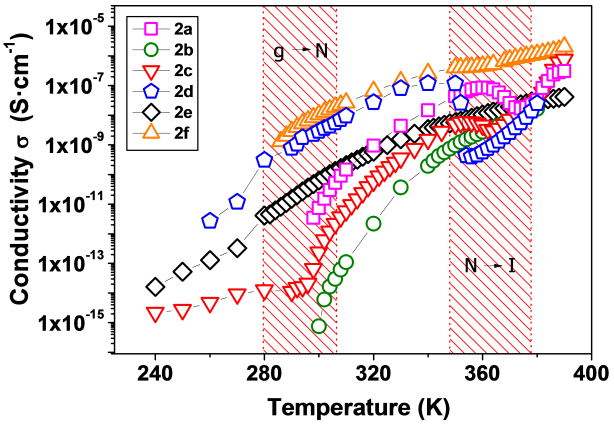


Figure 5. Plots of conductivity σ (S·cm$^{-1}$) *vs* temperature T (K). The σ values were extracted from the equivalent circuit fits. Temperature regions of phase transitions are indicated: glass to nematic mesophase (g → N) and nematic mesophase to isotropic liquid (N → I).

While the phase transition temperatures occur within a short range for all compounds **2a–2f**, Figure 5 shows several transitional features to different extents for the different compounds near the phase transitions. In all cases, an increase in conductivity is found as the temperature increases, and also with increasing structural mobility. At g → N transition most compounds show a perceptible increase in conductivity, which may be associated to the onset of ionic conductivity and favoured by structural flexibility and cooperative motions as mentioned above.[21]

All the compounds evolve towards more similar conductivities at higher temperature or in the isotropic liquid, but their conductivities are quite different at the initial mesophase stage. This is not in contradiction with our earlier conclusion that the counteranions hardly participate as charge carriers in the ionic conduction, because influence of the immobile anion on the mobility of the $K^+$ or $Li^+$ charge carriers is to be expected. In fact, the

counteranions (which, when located in LCs are usually close to the cations to stabilize the material by electrostatic interactions) have two possible influences producing different mobility of the $K^+$ or $Li^+$ charge carriers. One is obviously their electrostatic charge (-1, -2, -4) and their position in the mesophase relative to the cation in the crown; the other is the different diazacrown/anion ratios, changing from 1:1 in $I^-$ and $[AuCl_4]^-$ to 2:1 in $[PtCl_4]^{2-}$ and 50% $[AuCl_4]^-$, and finally 4:1 in $[Fe(CN)_6]^{4-}$. These changes mean that the cation mobility is occurring in a basically hydrophobic medium, apparently homogeneous that, however, contains in the proximity of the cation-crown position electrostatic fields created by the anions, which have different charges and different geometrical distributions from one compound to another (Figure 6).

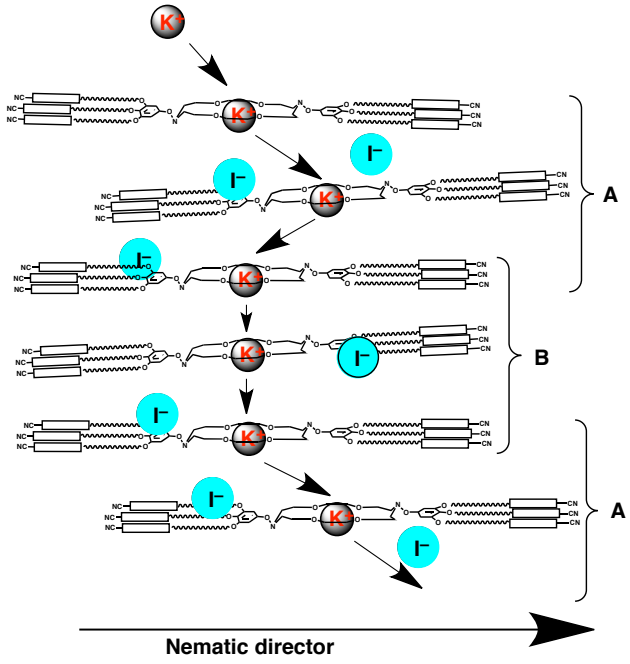


Figure 6. Two ways for K+ to move from one crown to a close one: **A**) When the crowns are not aligned, the cation moves along the nematic orientation to find another crown. Low energy paths for this are found with the help of elctrostatic interactions with the anions. **B**) When occasional momentaneous alignement is found, it facilitates the mobility.

Interestingly, as mentioned above, most compounds show a dip in the conductivity when entering into the isotropic liquid state at the N → I transition, a feature that is most prominently shown in Figure 5 by compounds **2a** and **2d**. This points out towards an ionic conduction mechanism in the mesophase that could use short-range temporary diaza-crown channels formed by stacking of a few units of diaza-crown moieties. Some percentage of alignments can statistically exist in a predominantly non-lamellar N mesophase, might be more easily achieved for short times when the mesophase becomes more fluid, and would disappear when the mesophase collapses at the N → I transition. It is worth reminding here the low enthalpy transition observed in the DSC studies, at the start of the clearing transition (similar temperatures as the dip in conductivity), which could correspond to the structural change of alignment/non-alignment of some crowns into short channels. Since this should correspond to a small percentage of the molecules in a non-lamellar mesophase, its enthalpy contribution must be small and it precedes the real clearing. This finding can be considered further evidence that the ionic conduction in the mesophase relies on the movement of the $M^+$ = $K^+$, $Li^+$ cations initially coordinated by the aza-crown heteroatoms at the corresponding molecular positions.

A further remarkable feature observed in Figure 5 is the higher conductivity in the mesophase of compound **2d** as compared to **2c**, by a factor of about 20. Both compounds possess a $K^+$ cation in the 18-diaza-crown ether and $AuCl_4^-$ counteranions in the mesophase, but the diazacrown/anion changes from 1:1 in **2c** to 2:1 in **2d**. Since this is the only difference between the two compositions and conduction is likely dominated by the $K^+$ cation as mentioned above, it is obvious that the existence of 18-diazacrown ether vacant sites acting in **2d** highly facilitates the ionic charge transport. This effect is well known in solid-state electrolytes, where the presence of defects or vacant sites, increase the mobility of ions.[22] Therefore, in 18-crown ether and similar materials the presence of vacant sites besides $K^+$ occupied sites may be a convenient strategy for increased ionic conductivity, as observed in **2d**. Curiously, in the isotropic liquid phase the two *σ vs. T* curves for **2d** and **2c** cross each other, possibly due to the higher charge carriers concentration in **2c** when the $AuCl_4^-$ counter anions join as charge carriers.[23] In other words, this behaviour points towards a cross-over from ionic conductivity in the mesophase, dominated by the cations at the molecular M = K, Li positions, to large contribution by additional species, possibly the counteranions, in the isotropic liquid. Finally, the use of a misfit small cation ($Li^+$) facilitates tremendously its mobility.

Selected ionic conductivity and activation energy data are summarised in Table 2 together with the activation energies extracted from the respective Arrhenius plots (ln *σ vs* 1/*T*). In order to compare these data with the literature, it should be noted that there are almost no examples of ionic conductivity on liquid crystals with potassium salts. Mesogenic complexes based on poly(ethyleneoxide) with $KCF_3SO_3$ display ionic conductivities around $10^{-3}$ S·cm$^{-1}$ in the range 100-150 °C, much higher than found in our system.[24] On the other hand, several works in the literature deal with lithium ionic conductivity in LCs. Our values of 4.01 $10^{-7}$ (350K) and 2.02 $10^{-6}$ S·cm$^{-1}$ (390K) are larger than those reported in carbonate-derived columnar liquid crystal ($10^{-8}$ S·cm$^{-1}$),[25] but smaller than in carbonate-derived SmA mesophases ($10^{-6}$-$10^{-4}$ S·cm$^{-1}$)[26] or in zwitterionic liquid crystals ($10^{-5}$-$10^{-4}$ S·cm$^{-1}$).[27]

Table 2: Ionic conductivities and activation energies in the mesophase (350 K), and ionic conductivities as isotropic liquid (390 K) for compounds **2a**-**2f**.

| Compound | σ at 350K/S·cm$^{-1}$ | σ at 390 K/ S·cm$^{-1}$ | $E_A$ (mesophase) (eV-Kcal/mol) |
|---|---|---|---|
| **2a** | 4.37 10$^{-8}$ | 3.09 10$^{-7}$ | 1.16-26.7 |
| **2b** | 9.67 10$^{-10}$ | 1.64 10$^{-8}$ * | 1.02-23.5 |
| **2c** | 4.87 10$^{-9}$ | 7.76 10$^{-7}$ | 1.70-39.1 |
| **2d** | 1.18 10$^{-7}$ | 7.62 10$^{-7}$ | 0.95-21.8 |
| **2e** | 5.81 10$^{-9}$ | 4.19 10$^{-8}$ | 0.63-14.5 |
| **2f** | 4.01 10$^{-7}$ | 2.02 10$^{-6}$ | 0.74-17.0 |

* The maximum value of ionic conductivity was measured at 380 K.

The activation energies in the mesophase, $E_A$, are in the range of 0.63–1.70 eV, which can be considered typical values for ionically conducting materials.[21,28] More than that, they are in the order of magnitude (roughly 20-45 kcal mol$^{-1}$) of bonding interactions of $K^+$ or $Li^+$ to 18-crown-ether proposed in the scarce experimental[29] and theoretical[30] values reported in the literature. In spite of the difficulty to make correct estimations of the participation of solvation energies in the literature studies on the solvent, or of the anion coulombic field interactions modifying the cation mobility in our mesophases, we consider that this coincidence of the range ΔH values with that of crown-$K^+$ or crown $Li^+$ bonding interactions is an acceptable support of $K^+$, $Li^+$ as the charge carriers in our compounds in the mesophase, and fits well the image of this mobility as the cation jumping between crown moieties that are close by.

## Conclusions

A nematic liquid crystal based on a 18-diaza-crown ether macrocycle symmetrically equipped with six decylalkoxy cyanobiphenyl chains has been synthesised that is able to coordinate $K^+$ with different counteranions. This affords ionic macrocycles with mesogenic behaviour (N mesophase) and little thermal variation compared to the parent neutral macrocycle. The permittivity and conductivity studies on these potassium ionic liquid crystals support ionic conductivity in the mesophase, with $K^+$ as the charge carrier. In a basically unfriendly environment of aliphatic and aromatic zones we conceive the mobility of $K^+$ in the mesophase as a sequence of jumps from one crown to another close to it, involving bond breaking and making to the successive crowns. Some DSC observations are compatible with the possible formation of instantaneous short-range alignment of crowns into channels in the otherwise non-lamellar N phase.

In this model, the improvement in conductivity using $Li^+$ instead of $K^+$ (the corresponding LiI adduct is about 10 times more conducting than KI) is due to the smaller activation energy required to break the $M^+$-crown interactions. In the same model, unoccupied crown positions into the mixture should facilitate the carrier mobility and our measurements confirm that the conductivity becomes 20 times higher when the metallo-crown ILC material is doped with the organic empty-crown molecules.

## Experimental Section

IR spectra were recorded on a Frontier Perkin–Elmer spectrophotometer (4000–200 cm$^{-1}$) coupled to a Pike GladiATR-210 accessory. $^1$H NMR spectra were recorded on Bruker AV-400 (400.13 MHz) or Varian 500 (499.73 Hz) instruments in $CDCl_3$ solutions (if no other solvent is stated); chemical shifts are quoted relative to $SiMe_4$ (external, $^1$H). $^1$H NMR labels are in Figure 1. Elemental analyses were performed with a Perkin–Elmer 2400 microanalyzer. MALDI-TOF mass spectrometry was carried out in Bruker Autoflex instrument. Polarised Optical Microscopy (POM) was performed with a Leica DMRB microscope equipped with a hot stage Mettler Toledo FP 90. Differential Scanning Calorimetry was performed with a Perkin Elmer DSC-7 instrument calibrated with Indium as reference (mp: 156.6 °C, ΔH = 28.4 J/g) and water, the thermograms were recorded at 2°C/min. The X-ray diffractograms at variable temperature were recorded on a PANalytical X'Pert PRO MPD diffractometer with Cu-Kα (1.54 Å) radiation in the θ–θ configuration equipped with an Anton Paar HTK1200 heating stage. 3,4,5-trialkoxybenzoic acid compounds were prepared by literature methods.[13a]

### Dielectric measurements

All samples have been investigated by impedance spectroscopy in the range 160–390 K during heating and cooling cycles using a custom-made liquid measurement cell as reported previously.[21] The complex impedance was measured using an alternating voltage signal of 100 mV amplitud, in a frequency range of 1 Hz – 10 MHz. The temperature was increased by 20 K in temperature ranges where no phase transition would be expected. Approaching phase transitions the temperature increments would be adjusted to 10 K, 5 K and finally 2 K. Each temperature was stabilised for several minutes until an impedance spectrum was measured in terms of the real part of the impedance Z' and the imaginary part Z'' over the full frequency range. The temperature steps and the rather careful temperature stabilization imply that the samples were heated relatively slowly near the phase transitions, possibly considerably slower than the heating ramp for the DSC data taken previously. The complex impedance data (Z* = Z′ + iZ″) were converted into the complex conductivity σ* and capacitance C* notations, σ* = σ′ + iσ″ and C* = C′ – iC″, using the standard conversions: Z* = (gσ*)$^{-1}$ and Z* =

$(i\omega C^*)^{-1}$, where g (in cm) is the geometrical factor given by the electrode area divided by the electrode distance, and ω is the angular frequency. Due to experimental limitations g could only be estimated from the weight and density of the powder measured initially, and the measured cell dimensions. Equivalent circuit fitting of the dielectric data was performed by using commercial ZView software. The conductivity and permittivity values extracted from the equivalent circuit fits were plotted *versus* temperature, but only physically meaningful values with sufficiently low fitting errors (< 5%) were considered.

**Synthesis of compounds**

*Synthesis of compounds **1** and **2***: The compound 3,4,5-tridecyloxybenzoic acid (0.9 g, 1.52 mmol) was dissolved in 15 mL of dry DCM under argon atmosphere. After addition of oxalyl chloride (1.245 ml, 14 mmol) and DMF (catalytic amount), the mixture was stirred for 3h under reflux. The excess of oxalyl chloride and solvent were removed under vacuum. The acid chloride intermediate was then dried at 60 °C under vacuum for 24 h before being dissolved in 15 mL of dry THF. This solution was dropwise added to a 15 ml THF solution maintained at 0 °C and containing 1,4-diaza-18-crown-6 (0.19 g, 0.72 mmol) and triethylamine (0.3 ml, 2.13 mmol). The reaction mixture was allowed to warm up to room temperature and kept under stirring for overnight. The crude obtained after THF evaporation was purified by column chromatography (silica gel, DCM/MeOH 95:5). The desired product was then dried at 45 °C under vacuum. Compound **1** was obtained as a viscous orange solid. Yield: 0.807 g, 79%. $^1$H NMR (500 MHz, $CDCl_3$): δ 6.56 (4H, s, $H_{arom}$), 3.94 (12H, t, J = 6.5 Hz, O-$CH_2$), 3.82-3.71 (m, 8H, $CH_2$-N), 3.69-3.52 (m, 16H, O-C*H*$_2$-C*H*$_2$-O) 1.81-1.69 (12H, m, O-$CH_2$-C*H*$_2$), 1.51-1.18 (84H, m, $CH_3$-(C*H*$_2$)$_7$), 0.88 (18H, t, J = 6.7 Hz, $CH_3$); IR (in solid cm$^{-1}$): 1634 ($\nu_{c=o}$); MS (MALDI-TOF): *m/z*: calc (M = $C_{86}H_{154}N_2O_{12}$), $(M + H)^+$ 1408,16**;** found: 1408,3. Anal. calcd for $C_{86}H_{154}N_2O_{12}$: C 73.35, H 11.02, N 1.99; found C 73.43, H 11.29, N 1.99.

In a similar way, compound **2** was obtained as a yellow solid. Yield: 1.34 g, 61%. $^1$H NMR (500 MHz, $CDCl_3$): δ 7.70-7.58 (24H, m, H$^1$+H$^2$), 7.53-7.47 (12H, m, H$^3$), 7.01-6.93 (12H, m, H$^4$), 6.57 (4H, s, -$CH_{ar}$), 4.06-3.92 (24H, m, O-$CH_2$), 3.82-3.70 (8H, m, $CH_2$-N-) 3.69-3.52 (16H, m, O-C*H*$_2$-C*H*$_2$-O), 1.85-1.70 (24H, m, O-$CH_2$-C*H*$_2$), 1.51-1.25 (72H, m, (-$CH_2$-)$_6$). IR (in solid cm$^{-1}$): 2223 ($\nu_{C\equiv N}$), 1623 ($\nu_{c=o}$); MS (MALDI-TOF): *m/z*: calc (M = $C_{164}H_{196}N_8O_{18}$), $(M + H)^+$ 2566,47; found: 2566,5. Anal. calcd for $C_{164}H_{196}N_8O_{18}$: C 76.72, H 7.69, N 4.36; found C 76.44, H 7.9, N 4.23.

*Synthesis of adducts **1a-1b***: KI (4.7 mg, 0.028 mmol) or $K_2[PtCl_4]$ (7.4 mg, 0.018 mmol) in 5 ml deoxygenated MeOH were stirred under ultrasound irradiation during 15 minutes and then added to a solution of macrocycle **1** (for **1a** 40 mg, 0.028 mmol; for **1b** 50 mg, 0.036 mmol in 5 ml diethyl ether under $N_2$. The mixture was stirred overnight at 35 °C. The solution was filtered over celite and dried in vacuum. The products were obtained as waxy yellow (**1a**) or brown (**1b**).

Yield of **1a**: 40 mg, 89%. $^1$H NMR (400 MHz, $CDCl_3$): δ 6.57 (4H, s, $H_{arom}$), 3.94 (12H, t, J = 6.5 Hz, O-$CH_2$), 3.823-3.73 (8H, m, -$CH_2$-N), 3.69-3.51 (16H, m, $CH_2$-$CH_2$-O, $CH_2$-O) 1.82-1.69 (12H, m, O-$CH_2$-$CH_2$), 1.50-1.19 (84H, m, $CH_3$-(C$H_2$)$_7$), 0.88 (18H, t, J = 6.7 Hz, $CH_3$); IR (in solid,cm$^{-1}$): 1634 ($\nu_{c=o}$); MS (MALDI-TOF): *m/z*: calcd.(M = $C_{86}H_{154}N_2O_{12}$ macrocycle **1**), calcd.$(M + H)^+$: 1408,16; found: 1408,3; calcd.$(M + Na)^+$ 1430,14; found: 1430,3; calcd.$(M + K)^+$ 1446,11; found: 1446,1. Anal. calcd. for $C_{86}H_{154}N_2IKO_{12}$: C 65.62, H 9.86, N 1.78; found C 65.36, H 10.07, N 2.02. Yield of **1b**: 50 mg, 87%: $^1$H NMR (400 MHz, $CDCl_3$): δ 6.57 (4H, s, $H_{arom}$), 3.94 (12H, t, J = 6.5 Hz, O-$CH_2$), 3.82-3.72 (8H, m, -$CH_2$-N), 3.68-3.51 (16H, m, $CH_2$-$CH_2$-O, $CH_2$-O) 1.80-1.68 (12H, m, O-$CH_2$-$CH_2$), 1.51-1.18 (84H, m, $CH_3$-(C$H_2$)$_7$), 0.88 (18H, t, J = 6.6 Hz, $CH_3$); IR (in solid,cm$^{-1}$): 1634 ($\nu_{c=o}$); MS (MALDI-TOF): *m/z*: (M = $C_{86}H_{154}N_2O_{12}$ macrocycle **1**), calcd.$(M + H)^+$: 1408,16; found: 1408,3; calcd.$(M + Na)^+$ 1430,14; found: 1429,4; calcd. $(M + K)^+$ 1446,11; found: 1445,4. Anal. calcd. for $C_{172}H_{308}N_4Cl_4K_2O_{24}Pt$: C 63.93, H 9.61, N 1.73; found C 63.71, H 9.89, N 2.00.

*Synthesis of adducts **2a-2f***: $M_nA$ (KI 4.8 mg, 0.029 mmol, $K_2[PtCl_4]$ 7.0 mg, 0.017 mmol, $K[AuCl_4]$ 10.5 mg, 0.028 mmol, $K[AuCl_4]$ 5.3 mg, 0.014 mmol, $K_4[Fe(CN)_6]$ 3.0 mg, 0.007 mmol or LiI 3.4 mg, 0.025 mmol) in 5 ml dry dichloromethane was stirred under ultrasound irradiation during 15 minutes and then added to a solution of macrocycle **2** (for **2a** 75 mg, 0.029 mmol; for **2b** 86.6 mg, 0.034 mmol; for **2c**-**2d**-**2e** 72 mg, 0.028 mmol; for **2f** 64 mg, 0.025 mmol) in 3 ml dichloromethane under $N_2$. The mixture was stirred overnight at 35 °C. The solution was filtered over celite and dried in vacuum. The products were obtained as beige (**2a**), ligth yellow (**2b**, **2e**) grey (**2c**, **2d**) or yellow (**2f**) solids.

Yield of **2a**: 73 mg, 92%. $^1$H NMR (500 MHz, $CDCl_3$): δ 7.70-7.59 (24H, m, $H_1$, $H_2$), 7.54-7.48 (12H, m, $H_3$), 7.00-6.94 (12H, m, $H_4$), 6.57 (4H, s, -$CH_{ar}$), 4.06-3.92 (24H, m, O-$CH_2$), 3.82-3.71 (8H, m, -$CH_2$-N-), 3.69-3.52 (16H, m, O-C*H*$_2$-C*H*$_2$-O), 1.85-1.70 (24H, m, O-$CH_2$-C*H*$_2$-), 1.51-1.25 (72H, m, (-$CH_2$-)$_6$). IR (in solid cm$^{-1}$): 2224 ($\nu_{C\equiv N}$), 1631 ($\nu_{c=o}$); MS (MALDI-TOF): *m/z*: calc (M = $C_{164}H_{196}N_8O_{18}$ macrocycle **2**), calc $(M + H)^+$ 2566,47; found: 2566,5; calc $(M + Na)^+$: 2588,46; found: 2588,5; calc $(M + K)^+$: 2604,43; found: 2604,5. Anal. calcd for $C_{164}H_{196}N_8KIO_{18}$: C 72.06, H 7.23, N 4.10; found C 71.87, H 7.14, N 4.02.

Yield of **2b**: 80 mg, 85%. $^1$H NMR (500 MHz, $CDCl_3$): δ 7.71-7.58 (24H, m, $H_1$, $H_2$), 7.54-7.48 (12H, m, $H_3$), 7.00-6.93 (12H, m, $H_4$), 6.57 (4H, s, -$CH_{ar}$), 4.03-3.91 (24H, m, O-$CH_2$), 3.83-3.71 (8H, m, -$CH_2$-N-) 3.69-3.52 (16H, m, O-C*H*$_2$-C*H*$_2$-O), 1.84-1.68 (24H, m, O-$CH_2$-C*H*$_2$-), 1.51-1.18 (36H, m, (-$CH_2$-)$_6$). IR (in solid cm$^{-1}$): 2224 ($\nu_{C\equiv N}$), 1628 ($\nu_{c=o}$); MS (MALDI-TOF): *m/z*: calc (M = $C_{164}H_{196}N_8O_{18}$ macrocycle **2**), calc $(M + H)^+$ 2566,47; found: 2566,5; calc $(M + Na)^+$: 2588,46; found: 2588,5; calc $(M + K)^+$: 2604,43; found: 2604,5. Anal. calcd for $C_{328}H_{392}Cl_4K_2N_{16}O_{36}Pt$ : C 70.99, H 7.12, N 4.04; found C 70.83, H 7.17, N 3.90.

Yield of **2c**: 80 mg, 98%. $^1$H NMR (500 MHz, $CDCl_3$): δ 7.79-7.58 (24H, m, $H_1$, $H_2$), 7.57-7.44 (12H, m, $H_3$), 7.03-6.91

(12H, m, $H_4$), 6.57 (4H, s, -$CH_{ar}$), 4.09-3.88 (24H, m, O-$CH_2$), 3.82-3.71 (8H, m, -$CH_2$-N-) 3.67-3.48 (16H, m, O-C$H_2$-C$H_2$-O), 1.83-1.69 (24H, m, O-$CH_2$-C$H_2$-), 1.60-1.22 (72H, m, (-$CH_2$-)$_6$). IR (in solid $cm^{-1}$): 2223 ($\nu_{C\equiv N}$), 1628 ($\nu_{c=o}$); MS (MALDI-TOF): *m/z*: calc (M = $C_{164}H_{196}N_8O_{18}$ macrocycle **2**), calc $(M + H)^+$ 2566,47; found: 2566,5; calc $(M+Na)^+$: 2588,46; found: 2588.5; calc $(M+K)^+$: 2604,43: found 2604,5; calc ($AuCl_4^-$): 338.83; found: 338.9. Anal. calcd $C_{164}H_{196}AuCl_4KN_8O_{18}$: C 66.88, H 6.71, N 3.80; found C 67.11, H 7.00, N 3.69.

Yield of **2d**: 71 mg, 93%. $^1$H NMR (500 MHz, $CDCl_3$): δ 7.72-7.58 (24H, m, $H_1$, $H_2$), 7.55-7.48 (12H, m, $H_3$), 7.01-6.92 (12H, m, $H_4$), 6.57 (4H, s, -$CH_{ar}$), 4.05-3.89 (24H, m, O-$CH_2$), 3.86-3.72 (8H, m, -$CH_2$-N-) 3.71-3.49 (16H, m, O-C$H_2$-C$H_2$-O), 1.84-1.69 (24H, m, O-$CH_2$-$CH_2$-), 1.65-1.20 (72H, m, (-$CH_2$-)$_6$). IR (in solid $cm^{-1}$): 2221 ($\nu_{C\equiv N}$), 1631 ($\nu_{c=o}$); MS (MALDI-TOF): *m/z*: calc (M = $C_{164}H_{196}N_8O_{18}$ macrocycle **2**), calc $(M+H)^+$ 2566,47; found: 2567,5; calc $(M+Na)^+$: 2588,46; found: 2588.5; calc $(M+K)^+$: 2604,43; found: 2604,5. Anal. calcd for $C_{164}H_{196}Au_{0.5}Cl_2K_{0.5}N_8O_{18}$: C 71.46, H 7.17, N 4.07; found C 71.66, H 7.26, N 3.98.

Yield of **2e**: 70 mg, 93%. $^1$H NMR (500 MHz, $CDCl_3$): δ 7.77-7.57 (24H, m, $H_1$, $H_2$), 7.57-7.46 (12H, m, $H_3$), 7.06-6.90 (12H, m, $H_4$), 6.57 (4H, s, -$CH_{ar}$), 4.11-3.88 (24H, m, O-$CH_2$), 3.86-3.68 (8H, m, -$CH_2$-N-) 3.68-3.48 (16H, m, O-C$H_2$-C$H_2$-O), 1.91-1.68 (24H, m, O-$CH_2$-C$H_2$-), 1.66-1.17 (72H, m, (-$CH_2$-)$_6$). IR (in solid $cm^{-1}$): 2224, 2060 ($\nu_{C\equiv N}$), 1628 ($\nu_{c=o}$); MS (MALDI-TOF): *m/z*: calc (M = $C_{164}H_{196}N_8O_{18}$ macrocycle **2**), calc $(M + H)^+$ 2566,47; found: 2566,5; calc $(M+Na)^+$: 2589,46; found: 2588,5; calc $(M + K)^+$: 2604,43; found: 2604,4. Anal. calcd for $C_{662}H_{784}FeK_4N_{38}O_{72}$: C 74.74, H 7.43, N 5.00; found C 74.52, H 7.60, N 4.84.

Yield of **2f**: 67 mg, 97%. $^1$H NMR (500 MHz, $CDCl_3$): δ 7.72-7.56 (24H, m, $H_1$, $H_2$), 7.54-7.45 (12H, m, $H_3$), 7.02-6.89 (12H, m, $H_4$), 6.57 (4H, s, -$CH_{ar}$), 4.03-3.89 (24H, m, O-$CH_2$), 3.88-3.75 (8H, m, -$CH_2$-N-) 3.73-3.51 (16H, m, O-C$H_2$-C$H_2$-O), 1.86-1.69 (24H, m, O-$CH_2$-C$H_2$-), 1.64-1.23 (72H, m, (-$CH_2$-)$_6$). IR (in solid $cm^{-1}$): 2223 ($\nu_{C\equiv N}$), 1628 ($\nu_{c=o}$); MS (MALDI-TOF): *m/z*: calc (M = $C_{164}H_{196}N_8O_{18}$ macrocycle **2**), calc $(M + H)^+$ 2566,47; found: 2566,5; calc $(M + Li)^+$: 2572,48; found: 2572,6; calc $(M+Na)^+$: 2589,46; found: 2588.6. Anal. calcd for $C_{164}H_{196}N_8ILiO_{18}$: C 72.92, H 7.31, N 4.15; found C 72.63, H 7.44, N 4.13.

## Conflicts of interest

There are no conflicts to declare.

## Acknowledgements

We thank the Ministerio de Economía y Competitividad (Project CTQ2014-52796-P) for financial support. C. Cuerva is grateful to the Programa de Financiación de Universidad Complutense de Madrid-Santander Universidades (Spain), for his predoctoral contract.

## References

[1] T. Welton, Room-Temperature Ionic Liquids. Solvents for Synthesis and Catalysis, *Chem. Rev.,* 1999, **99**, 2071.

[2] a) T. Welton, Ionic liquids in catalysis, *Coord. Chem. Rev.,* 2004, **248**, 2459; b) N.V. Plechkova and K. R. Seddon, Applications of ionic liquids in the chemical industry, *Chem. Soc. Rev.,* 2008, **37**, 123; c) M. Watanabe, M. L. Thomas, S. Zhang, K. Ueno, T. Yasuda and K. Dokko, Application of Ionic Liquids to Energy Storage and Conversion Materials and Devices, *Chem. Rev,.* 2017, **117**, 7190.

[3] K. Goossens, K. Lava, C. W. Bielawski and K. Binnemans, Ionic Liquid Crystals: Versatile Materials, *Chem. Rev.*, 2016, **116**, 4643.

[4] a) M. Yoshio and T. Kato, Liquid Crystals as Ion Conductors. In Handbook of Liquid Crystals, Vol. 8: Applications of Liquid Crystals, 2nd ed.; J. W. Goodby, P. J. Collings, T. Kato, C. Tschierske, H. Gleeson and P. Raynes, Eds.; Wiley-VCH: Weinheim, 2014; pp 727; b) M. Armand, F. Endres, D. R. MacFarlane, H. Ohno and B. Scrosati, Ionic-Liquid Materials for the Electrochemical Challenges of the Future, *Nat. Mater.,* 2009, **8**, 621; c) T. Ohtake, M. Ogasawara, K. Ito-Akita, N. Nishina, S. Ujiie, H. Ohno and T. Kato, Liquid-Crystalline Complexes of Mesogenic Dimers Containing Oxyethylene Moieties With $LiCF_3SO_3$: Self-Organized Ion Conductive Materials, *Chem. Mater.,* 2000, **12**, 782; d) K. Kishimoto, Y. Sagara, T. Kato, T. Mukai, H. Ohno and N. Tamaoki, Two Dimensionally Ion-Conductive Liquid Crystals of Cholesterol/Tetra(Ethylene Oxide) Block Molecules, *Mol. Cryst. Liq. Cryst.*, 2005, **435**, 777.

[5] a) K. Isoda, T. Yasuda, M. Funahashi and T. Kato, Redox-Active (Electrochromic) Liquid Crystals, in Handbook of Liquid Crystals, Vol. 8: Applications of Liquid Crystals, 2nd ed.; J. W. Goodby, P. J. Collings, T. Kato, C. Tschierske, H. Gleeson and P. Raynes, Eds.; Wiley-VCH: Weinheim, 2014; pp 709; b) K. Binnemans and C. Görller-Walrand, Lanthanide-Containing Liquid Crystals and Surfactants, *Chem. Rev.,* 2002, **102**, 2303; c) T. D. Do and A. R. Schmitzer, Intramolecular Diels Alder Reactions in Highly Organized Imidazolium Salt-Based Ionic Liquid Crystals, *RSC Adv.,* 2015, **5**, 635.

[6] a) M. Moshkovich, Y. Gofer and D. Aurbach, Investigation of the Electrochemical Windows of Aprotic Alkali Metal (Li, Na, K) Salt Solutions, *J. Electrochem. Soc.,* 2001, **148**, E155; b) E. Cho, J. Mun, O. B. Chae, O. M. Kwon, H.-T. Kim, J. H. Ryu, Y. G. Kim and S. M. Oh, Corrosion/Passivation of Aluminum Current Collector in Bis (Fluorosulfonyl) Imide-Based Ionic Liquid for Lithium-Ion Batteries, *Electrochem. Commun.,* 2012, **22**, 1; c) X. Wu, D. P. Leonard and X. Ji, Emerging Non-Aqueous Potassium-Ion Batteries: Challenges and Opportunities, *Chem. Mater.,* 2017, **29**, 5031; d) K. Lei, F. Li, C. Mu, J.

Wang, Q. Zhao, C. Chen and J. Chen, High K-Storage Performance Based on the Synergy of Dipotassium Terephthalate and Ether-Based Electrolytes, *Energy Environ. Sci.*, 2017, **10**, 552; e) G. He, L. F. Nazar, Crystallite Size Control of Prussian White Analogues for Non-Aqueous Potassium-Ion Batteries, *ACS Energy Lett.,* 2017, **2**, 1122.

[7] (a) C. J. Pedersen, The Discovery of Crown Ethers (Nobel Leture), *Angew. Chem., Int. Ed. Engl.,* 1988, **27**, 1021; b) C. J. Pedersen, Cyclic Polyethers and their Complexes with Metal Salts, *J. Am. Chem. Soc.,* 1967, **89**, 7017; c) G. W. Gokel, W. M. Leevy and M. E. Weber, *Chem. Rev.,* 2004, **104**, 2723.

[8] a) M. Kaller and S. Laschat, Liquid crystalline crown ethers, *Top Curr Chem.,* 2011, **318**, 109; b) M. Kaller, A. Baro and S. Laschat, Liquid crystal crown ethers and related compounds, in Handbook of liquid crystals, Vol. 6: Nanostructured and Amphiphilic Liquid Crystals; 2nd ed.; J. W. Goodby, P. J. Collings, T. Kato, C. Tschierske, H. Gleeson and P. Raynes, Eds.; Wiley-VCH: Weinheim, 2014; pp. 335.

[9] a) G. X. He, F. Wada, K. Kikukawa, S. Shinkai and T. Matsuda, Syntheses and Thermal Properties of New Liquid Crystals Bearing a Crown Ether Ring: Cation Binding in the Nematic Phase, *J. Org. Chem.,* 1990, **55**, 541; b) G. Johansson, V. Percec, G. Ungar, D. Abramic, Molecular recognition directed self-assembly of tubular liquid crystalline and crystalline supramolecular architectures from taper shaped (15-crown-5)methyl 3,4,5-tris(*p*-alkyloxybenzyloxy)benzoates and (15-crown-5)methyl 3,4,5-tris(*p*-dodecyloxy)benzoate, *J. Chem. Soc., Perkin Trans.,* 1994, **1**, 447; (c) V. Percec, G. Johansson, G. Ungar, J.P. Zhou, Fluorophobic Effect Induces the Self-Assembly of Semifluorinated Tapered Monodendrons Containing Crown Ethers into Supramolecular Columnar Dendrimers Which Exhibit a Homeotropic Hexagonal Columnar Liquid Crystalline Phase, *J. Am. Chem. Soc.*, 1996, **118**, 9855; (d) V. Percec, W. D. Cho, G. Ungar and D. J. P. Yeardley, Synthesis and NaOTf Mediated Self-Assembly of Monodendritic Crown Ethers, *Chem. Eur. J.*, 2002, **8**, 2011; (e) N. Steinke, W. Frey, A. Baro, S. Laschat, C. Drees, M. Nimtz, C. Hägele, F. Giesselmann, Columnar and Smectic Liquid Crystals Based on Crown Ethers, *Chem. Eur. J.,* 2006, **12**, 1026; f) N. Steinke, M. Jahr, M. Lehmann, A. Baro, W. Frey, S. Tussetschläger, S. Sauer and S. Laschat, Crown Ethers with Lateral Ortho-Terphenyl Units: Effect of Ester Groups and Sodium Salts on the Mesomorphic Properties, *J. Mater. Chem.,* 2009, **19**, 645. g) R.D Shannon, Revised effective ionic radii and systematic studies of interatomic distances in halides and chalcogenides, *Acta Cryst.*; **1976**, *A32*, 751.

[10] J. Arias, M. Bardají and P. Espinet, Palladium(II) metallomesogens of crown ether derivatized imines, and their sodium adducts. *J. Organomet. Chem.,* 2006, **691**, 4990; b) J. Arias, M. Bardají and P. Espinet, Luminescence and Mesogenic Properties in Crown-Ether-Isocyanide or Carbene Gold(I) Complexes: Luminescence in Solution, in the Solid, in the Mesophase, and in the Isotropic Liquid State, *Inorg. Chem.*, 2008, **47**, 3559; c) S. Coco, C. Cordovilla, P. Espinet, J.-L. Gallani, D. Guillon, and B. Donnio. Supramolecular Aggregates in Fluid Phases: Mesomorphic Orthopalladated Complexes with Substituted-Crown-Ethers and their Potassium adducts, *Eur. J. Inorg. Chem.,* 2008**,** 1210. d) N. Steinke, M. Kaller, M. Nimtz, A. Baro and S. Laschat, Columnar Liquid Crystals Derived from Crown Ethers with Two Lateral Ester-Substituted ortho-terphenyl Units: Unexpected Destabilisation of the Mesophase by Potassium Iodide, *Liq. Cryst.,* 2010, **37**, 1139; i) S. Laschat, A. Baro, T. Wöhrle and J. Kirres, Playing with nanosegregation in discotic crown ethers: from molecular design to OFETs, nanofibers and luminescent materials, *Liq. Cryst. Today*, 2016, **25**, 48.

[11] J. A. Schröter, C. Tschierske, M. Wittenberg and J. H. Wendorff, Liquid Crystalline Crown Ether: Forming Columnar Mesophases by Molecular Recognition, *Angew. Chem.,* 1997, **109**, 1160–1163; *Angew. Chem. Int. Ed. Engl.,* 1997, **36**, 1119–1121; b) M. Kaller, S. Tussetschläger, P. Fischer, C. Deck, A. Baro, F. Giesselmann, and S. Laschat, Columnar Mesophases Controlled by Counterions in Potassium Complexes of Dibenzo[18]crown-6 Derivatives, *Chem. Eur. J.*, 2009, **15**, 9530; c) M. Kaller, C. Deck, A. Meister, G. Hause, A. Baro amd S. Laschat, Counterion Effects on the Columnar Mesophases of Triphenylene- Substituted [18]Crown-6 Ethers: Is Flatter Better?, *Chem. Eur. J.,* 2010, **16**, 6326.

[12] A. Kwun-Wa Chan, K. Man-Chung Wong, V. W-W. Yam, Supramolecular Assembly of Isocyanorhodium(I) Complexes: AnInterplay of Rhodium(I)···Rhodium(I) Interactions, Hydrophobic−Hydrophobic Interactions, and Host−Guest Chemistry *J. Am. Chem. Soc*. 2015, **137**, 6920.

**[13]** a) Y. Molard, F. Dorson, V. Cîrcu, T. Roisnel, F. Artzner and S. Cordier, Clustomesogens: Liquid Crystal Materials Containing Transition-Metal Clusters, *Angew. Chem., Int. Ed.,* 2010, **49**, 3351; b) Y. Molard, A. Ledneva, M. Amela-Cortes, V. Cîrcu, N. G. Naumov, C. Mériadec, F. Artzner and S. Cordier, Ionically Self-Assembled Clustomesogen with Switchable Magnetic/Luminescence Properties Containing $[Re_6Se_8(CN)_6]^{n-}$ ($n$ = 3, 4) Anionic Clusters, *Chem. Mater*., 2011, **23**, 5122; c) A. S. Mocanu, M. Amela-Cortes, Y. Molard, V. Cîrcu and S. Cordier, Liquid Crystal Properties Resulting From Synergetic Effects Between Non-Mesogenic Organic Molecules and a One Nanometre Sized Octahedral Transition Metal Cluster, *Chem. Commun.*, 2011, **47**, 2056; d) M. Amela- Cortes, F.

Dorson, M. Prévôt, A. Ghoufi, B. Fontaine, F. Goujon, R. Gautier, V. Cîrcu, C. Mériadec, F. Artzner, H. Folliot, S. Cordier and Y. Molard, Thermotropic Luminescent Clustomesogen Showing a Nematic Phase: A Combination of Experimental and Molecular Simulation Studies, *Chem. Eur. J.,* 2014, **20**, 8561; e) V. Cîrcu, Y. Molard, M. Amela-Cortes, A. Bentaleb, P. Barois, V. Dorcet and S. Cordier, From Mesomorphic Phosphine Oxide to Clustomesogens Containing Molybdenum and Tungsten Octahedral Cluster Cores, *Angew. Chem., Int. Ed.,* 2015, **54**, 10921; f) Y. Molard, Clustomesogens: Liquid Crystalline Hybrid Nanomaterials Containing Functional Metal Nanoclusters, *Acc. Chem. Res.,* 2016, **49**, 1514.

[14] a) S. K. Nayak, M. Amela-Cortes, C. Roiland, S. Cordier and Y. Molard, From metallic cluster-based ceramics to nematic hybrid liquid crystals: a double supramolecular approach, *Chem. Commun.,* 2015, **51**, 3774; b) S. K. Nayak, M. Amela-Cortes, M. M. Neidhardt, S. Beardsworth, J. Kirres, M. Mansueto, S. Cordier, S. Laschat and Y. Molard, Phosphorescent columnar hybrid materials containing polyionic inorganic nanoclusters, *Chem. Commun.,* 2016, **52**, 3127.

[15] S. Igawa and S. Nakamura, Discotic liquid-crystalline crown ether derivatives and solid electrolytes therefrom, JP 2001172268 A, 2001.

[16] M. Benouazzane, S. Coco, P. Espinet, J. M. Martin-Alvarez, Liquid Crystals based on Halogold(I) Complexes with 4-Isocyano-4'-alkoxybiphenyl Derivatives, *J. Mater. Chem.*, 1995, **5**, 441.

[17] E. D. Glendening, D. Feller, and M. A. Thompson, An ab Initio Investigation of the Structure and Alkali Metal Cation Selectivity of 18-Crown-6, *J. Am. Chem. Soc.* 1994,**116**, 10657.

[18] C. Cuerva, J. A. Campo, M. Cano and R. Schmidt, Nanostructured discotic Pd(II) metallomesogens as one-dimensional proton conductors, *Dalton Trans.,* 2017, **46**, 96.

[19] Y. Shi, Y. Wang, M. Zhang, X. Dong, Influences of cation charge density on the photovoltaic performance of dye-sensitized solar cells: lithium, sodium, potassium, and dimethylimidazolium, *Phys. Chem. Chem. Phys.,* 2011, **13**, 14590.

[20] M. Okoshi, Y. Yamada, S. Komaba, A. Yamada and H. Nakai, Theoretical Analysis of Interactions between Potassium Ions and Organic Electrolyte Solvents: A Comparison with Lithium, Sodium, and Magnesium Ions, *J. Electrochem. Soc.,* 2017, **164**, A54. See also ref. 9g.

[21] C. Cuerva, J. A. Campo, M. Cano, J. Sanz, I. Sobrados, V. Diez-Gómez, A. Rivera-Calzada and R. Schmidt, Water-Free Proton Conduction in Discotic Pyridylpyrazolate-based Pt(II) and Pd(II) Metallomesogens, *Inorg. Chem.,* 2016, **55**, 6995.

[22] a) X. Liu, T. S. Bjørheim and R. Haugsrud, Defects formation and their effects on hydride ion transport properties in a series of $K_2NiF_4$-type oxyhydrides**,** *J. Mater. Chem. A*, 2018, **6**, 1454; b) S. B. R. S. Adnan, F. M. Salleh, N. S. Mohamed, Effect of interstitial $Li^+$ ion and vacant site $Li^+$ ion on the properties of novel $Li_{2.05}ZnAl_{0.05}Si_{0.95}O_4$ and $Li_{1.95}Zn_{0.95}Cr_{0.05}SiO_4$ ceramic electrolytes, Ceram. Int., 2016, **42**, 17941.

[23] P. Bonhôte, A. -P. Dias, N. Papageorgiou, K. Kalyanasundaram, M. Grätzel, Hydrophobic, Highly Conductive Ambient-Temperature Molten Salts, *Inorg. Chem.,* 1996, **35**, 1168.

[24] T. Ohtake, Y. Takamitsu, K. Ito-Akita, K. Kanie, M. Yoshizawa, T. Mukai, H. Ohno and T. Kato, Liquid-Crystalline Ion-Conductive Materials: Self-Organization Behavior and Ion-Transporting Properties of Mesogenic Dimers Containing Oxyethylene Moieties Complexed with Metal Salts, *Macromolecules,* 2000, **33***,* 8109.

[25] H. Shimura, M. Yoshio, A. Hamasaki, T. Mukai, H. Ohno and T. Kato, Electric Field Responsive Lithium Ion Conductors of Propylenecarbonate Based Columnar Liquid Crystals, *Adv. Mater.,* 2009, **21**, 1591.

[26] J. Sakuda, E. Hosono, M. Yoshio, T. Ichikawa, T. Matsumoto, H. Ohno, H. Zhou and T. Kato, Liquid-Crystalline Electrolytes for Lithium-Ion Batteries: Ordered Assemblies of a Mesogen-Containing Carbonate and a Lithium Salt, *Adv. Funct. Mater.,* 2015, **25**, 1206.

[27] B. Soberats, M. Yoshio, T. Ichikawa, H. Ohno and T. Kato, Zwitterionic liquid crystals as 1D and 3D lithium ion transport media, *J. Mater. Chem. A*, 2015, **3**, 11232.

[28] J. Prado-Gonjal, R. Schmidt, J. Espíndola-Canuto, P. Ramos-Alvarez and E. Morán, Increased ionic conductivity in microwave hydrothermally synthesized rare-earth doped ceria $Ce_{1-x}RE_xO_{2-(x/2)}$, *J. Power Sources*, 2012, **209**, 163.

[29] (a) H.-J. Buschmann, The Complexation of Alkali Metal Ions by Crown Ethers, Aza Crown Ethers, and Cryptands in Propylene Carbonate, *J. Incl. Phenom. Mol. Recognit. Chem.*, 1989, **7**, 581; (b) R. M. Izatt, R. E. Terry, B. L. Haymore, L. D. Hansen, N. K. Dalley, A. G. Avondet, and J. J. Christensen, Calorimetric Titration Study of the Interaction of Several Uni- and Bivalent Cations with 15-Crown-5, 18-Crown-6, and Two Isomers of Dicyclohexo-18-crown-6 in Aqueous Solution at 25 °C and μ = 0.1, *J. Am. Chem. Soc.*, 1976, **98**, 7620; (c) R. De Jong, and D. N. Reinhoudt, Stability and Reactivity of Crown-Ether Complexes, *Adv. Phys. Org. Chem.*, 1980, **17**, 279; (d) R. M. Izatt, J. S. Bradshaw, S. A. Nielsen, J. D. Lamb, J. J. Christensen and D. Sen, Thermodynamic and Kinetic Data for Cation-Macrocycle Interaction, *Chem. Rev.*, 1985, **85**, 271.

[30] Estimates for the binding enthalpies of the $K^+$/18C6 complexes close to 65 kcal $mol^{-1}$ are stronger, by about (30 kcal $mol^{-1}$ than experimentally determined values. E.

D. Glendening, D. Feller and Mark A. Thompson, An ab Initio Investigation of the Structure and Alkali Metal Cation Selectivity of 18-Crown-6, *J. Am. Chem. Soc.,* 1994, **116**, 10657, and references therein.